ИНСТИТУТ ЯДЕРНОЙ ФИЗИКИ СО АН СССР

V.F. Dmitriev, V.B. Telitsin

THEORETICAL ANALYSIS OF (e, e′N) and (γ, N) REACTIONS ON ^{16}O

PREPRINT 88-15

НОВОСИБИРСК

Theoretical Analysis of $(e, e'N)$ and (γ, N) Reactions on ^{16}O

V.F. Dmitriev, V.B. Telitsin

Institute of Nuclear Physics
630090, Novosibirsk, USSR

ABSTRACT

Random phase approximation in continuum with effective forces has been used to calculate the cross-sections of (γ, N) and $(e, e'N)$ reactions on oxigen nucleus. The spectra of nucleons and their angular correlations are calculated. The comparison with experimental data was performed revealing importance of more complex than $1p-1h$ configurations contribution.

1. INTRODUCTION

With modern electron accelerators and development of a method of an internal target in electron storage ring [1] there appeared a possibility of coincidence experiments not only at high momentum transfer where quasi-free scattering dominates [2] but at lower momentum transfer as well where giant resonanses (GR) and even isolated levels can be excited [3].

In this region of momentum transfer the $(e, e'N)$ reaction is close in kinematics to (γ, N) reaction and their comparison can be useful for study of nuclear structure. From the other hand there is a difference since the momentum of a virtual γ-quantum in $(e, e'N)$ reaction is several times greater than the momentum of a real γ-quantum in the (γ, N) reaction. In this case the GR with multipolarities higher than the dipole ones can be excited. In addition, the possibility of study 0^+-strength exist for electron scattering, the possibility that absents for the (γ, N) reaction.

For these reasons it is interesting to analyse together $(e, e'N)$ and (γ, N) reactions. We have chosen for the analysis an oxigen nucleus where the cross-section of (γ, N) reaction was measured starting from threshold up to the end of resonance region [4] and the data on $(e, e'N)$ reaction at $q \approx 0.5$ fm^{-1} appeared recently [5].

The structure of GR is determined by a superposition of $1p-1h$ states. In light nuclei the number of such states is relatively small. For example, for giant dipole resonance in ^{16}O there are 5 states for protons and 5 for neutrons. At small collectivity the rearrangement

of strength into collective peak is not complete. Considerable part of the strength remains in separate $1p-1h$ states. Effects of coupling of GR and $2p-2h$ configurations give rise fragmentation instead of spreading width. The escape width becomes comparatively large and must be taken into account explicitly in all theoretical calculations.

There exist several approaches to take into account the single-particle continuum. One of them is based on explicit separation of continuum states space. In this approach the system of equations can be formulated coupling the reaction channels and internal nuclear states [6, 7]. This approach is closely related to Feshbach's idea of doorway states [8]. It is rather general approach capable to describe emission of not only single nucleons but complex particles like d, t, ^{3}He as well. In practice, however, the system of equations for more than one type of emitted particles is very combersome and time consuming.

In other approaches the single-particle continuum is taken into account using coordinate representation. We can refer here to the papers of Bologna group [9] and to papers of Speth an co-workers [10, 11]. In [9] the system of integro-differential equations for $1p-1h$ self-consistent RPA amplitudes is formulated in coordinate space. In [10, 11] the equations for RPA transition-densities are formulated in the coordinate space and the Fourier-Bessel method is used to solve the equations.

Our approach is based on paper [12] and we used it before to analyse the influence of spin-orbit interaction on magnetic properties of nuclei [13]. In this paper using the mentioned approach we formulate and solve the equations for effective electromagnetic fields necessary for calculations of the cross-sections (parts 2 and 3). The results of calculations of (γ, N) and $(e, e'N)$ cross-sections are discussed in part 4.

2. THE CROSS-SECTIONS OF $(e, e'N)$ AND (γ, N) REACTIONS

2.1. Kinematics of the Processes

Let us start with useful kinematical relations and description of the coordinate system we shall use below. In Fig. 1 the diagramm of $(e, e'N)$ process is shown. The $p_\mu=(E, \vec{p})$ and $p'_\mu=(E', \vec{p}')$ are the four-momentum of initial and final electrons. The energy-momentum of gamma-quantum q_μ is $q_\mu=(\omega, \vec{q})=p_\mu-p'_\mu$. In ultra-

relativistic case one has

$$q^2=\omega^2-\vec{q}^{\,2}=-4EE'\sin^2(\theta/2), \tag{2.1}$$

where θ is the electron scattering angle in lab. system. The p_i, p_f and k are the momenta of initial, final nucleus and emitted nucleon. In the lab. system one has $p_{i\mu}=(M_i, 0)$, $p_{f\mu}=\left(M_f+E^*+\frac{(\vec{q}-\vec{k})^2}{2M_f}, \vec{q}-\vec{k}\right)$, where M_i and M_f are the masses of initial and final nucleus and E^* is the excitation energy of the final nucleus.

For description of angular distributions we shall use the coordinate system with the axes shown in Fig. 1. The orts are $\vec{e}_z=\frac{\vec{q}}{|\vec{q}|}$, $\vec{e}_y=\frac{\vec{q}\times\vec{p}}{|\vec{q}\times\vec{p}|}$ and $\vec{e}_x=\vec{e}_y\times\vec{e}_z$. Our coordinate system is the same as used in the de Forest's paper [14] and differs from those used in [15]. The last one is 90° rotated around z-axis relative to our system.

2.2. Cross-Sections

The amplitude of $(e, e'N)$ reaction in Born approximation is

$$T_{fi}=\frac{e^2}{q^2}\bar{u}(p')\gamma_\mu u(p) J_\mu(q) \tag{2.2}$$

where $J_\mu(q)=(\rho(q), \vec{J}(q))$ is matrix element of electromagnetic current. The $u(p)$ is the solution of free Dirac equation. The distortion due to electric field of a nucleus can be neglected for light nuclei where $Z\alpha\ll 1$.

For the cross-section differential in energy transfer and angles of scattered electron and emitted nucleon one has

$$\frac{d^3\sigma}{d\omega\, d\Omega\, d\Omega_k}=\sigma_M\frac{1}{(2\pi)^3}\,\frac{1}{4EE'\cos^2\frac{\theta}{2}}\left(\overline{|PJ|}^2+q^2\overline{|J|}^2\right)\frac{mk}{1-\frac{m}{M_f}\frac{q}{k}\cos\theta_k}, \tag{2.3}$$

where

$$\sigma_M=\frac{\alpha^2\cos^2\frac{\theta}{2}}{4E^2\sin^4\frac{\theta}{2}} \tag{2.4}$$

is the Mott cross-section, $P_\mu=p_\mu+p'_\mu$, m is reduced mass of emitted

nucleon, θ_k is the angle between $\vec{q}$ and $\vec{k}$. The bar means averaging over initial and summation over final nuclear states.

The cross-section (2.3) is written in lab. system. However, it is convenient to calculate the invariant expression in brackets in the center of mass system of final particles where the matrix element of nuclear current is well defined.

Taking into account the transversality of electromagnetic current one gets for the cross-section [15, 16]

$$\frac{d^3\sigma}{d\omega\, d\Omega\, d\Omega_k} = \sigma_M \frac{1}{(2\pi)^3}\left[\frac{W^2}{M_i^2} V_L(\theta)\, \overline{|\rho(q)|^2} + \right.$$

$$+ \frac{W}{M_i} V_{LT}(\theta)\ \mathrm{Re}\left[\overline{\rho(q)\cdot(J_+(q) - J_-(q))|} + V_T(\theta)\,(\overline{|J_+(q)|^2} + \overline{|J_-(q)|^2}) - \right.$$

$$\left.\left. - V_{TT}(\theta)\, 2\,\mathrm{Re}\,(\overline{J_+^*(q)\cdot J_-(q)})\right]\right] \frac{mk}{1 - \frac{m}{M_i}\frac{q}{k}\cos\theta_k}, \qquad (2.5)$$

where

$$V_L(\theta) = \frac{(q_\mu^2)^2}{(\vec{q}^{\,2})^2}; \qquad (2.6)$$

$$V_{LT}(\theta) = -\frac{q_\mu^2}{\vec{q}^{\,2}}\,\frac{E+E'}{|\vec{q}|}\,\mathrm{tg}^2\frac{\theta}{2}; \qquad (2.7)$$

$$V_T(\theta) = \mathrm{tg}^2\frac{\theta}{2} - \frac{q_\mu^2}{2\vec{q}^{\,2}}; \qquad (2.8)$$

$$V_{TT}(\theta) = -\frac{q_\mu^2}{2\vec{q}^{\,2}}; \qquad (2.9)$$

W/M_i is kinematical factor appeared due to transformation into center of mass system [15], $W^2 = M_i^2 + 2M_i\omega + q_\mu^2$; the circular components of a nuclear current are defined in a standard way [17]

$$J_\pm(q) = \vec{J}\cdot\vec{e}_\pm = \mp\frac{J_x \pm i J_y}{\sqrt{2}}. \qquad (2.10)$$

For the (γ, N) reaction one can find expression similar to (2.5). The recoil of a nucleus can be neglected for photo-reaction. For polarized gamma-quanta the differential cross-section is

$$\frac{d\sigma}{d\Omega_k} = \frac{\alpha}{4\pi}\,\frac{mk}{\omega}\left[\overline{|J_+|^2} + \overline{|J_-|^2} + \xi_2(\overline{|J_-|^2} - \overline{|J_+|^2}) - \right.$$

$$\left. - \xi_3\, 2\,\mathrm{Re}\,(\overline{J_+\cdot J_-^*}) - \xi_1\, 2\,\mathrm{Im}\,(\overline{J_+\cdot J_-^*})\right], \qquad (2.11)$$

where ξ_1, ξ_2, ξ_3 are the Stocks parameters of the density matrix of gamma-quanta [18]. In neglection of parity-violation effects the cross-section (2.11) does not depend on circular polarization parameter ξ_2. Furthermore, choosing the x-axis along one of the main axes of polarization density matrix one can omit the parameter ξ_1 or ξ_3. Finally (2.11) can be written as

$$\frac{d\sigma}{d\Omega_k} = \frac{\alpha}{4\pi}\,\frac{mk}{\omega}\left[(\overline{|J_+|^2} + \overline{|J_-|^2})\,V_T^{ph} - V_{TT}^{ph}\cdot 2\,\mathrm{Re}\,(\overline{J_+\cdot J_-^*})\right], \qquad (2.12)$$

where $V_T^{ph} = 1$ and $V_{TT}^{ph} = \xi_3$.

2.3. Multipole Expansion of Nuclear Electromagnetic Current

In (2.5) and (2.12) we have matrix elements of the Fourier-components of nuclear electromagnetic current:

$$\rho(q) = \int d^3r\, \rho(\vec{r})\, e^{i\vec{q}\vec{r}},$$

$$J_\lambda(q) = \int d^3r\, J_\lambda(\vec{r})\, e^{i\vec{q}\vec{r}}. \qquad (2.13)$$

There are several variants of multipole expansion that differs in definitions of multipole transition operators. We shall use the following definition:

$$\rho(q) = (4\pi)^{1/2} \sum_{J=0}^{\infty} i^J (2J+1)^{1/2}\, T_J^C(q), \qquad (2.14)$$

$$J_\lambda(q) = -(2\pi)^{1/2} \sum_{J=1}^{\infty} i^J (2J+1)^{1/2} (T_{J\lambda}^E(q) + \lambda T_{J\lambda}^M(q)), \quad (\lambda = \pm 1), \qquad (2.15)$$

where Coulomb, electric, and magnetic multipole transition operators are:

$$T_J^C(q) = \int d^3r\, \rho(\vec{r})\, j_J(qr)\, Y_{J0}(\hat{r}); \qquad (2.16)$$

$$T_{J\lambda}^E(q) = \frac{1}{q}\int d^3r\, j_J(qr)\, \vec{Y}_{J\lambda}^J(\hat{r})\cdot \mathrm{rot}\,\vec{j}(\vec{r}); \qquad (2.17)$$

$$T_{J\lambda}^M(q) = \int d^3r\, j_J(qr)\, \vec{Y}_{J\lambda}^J(\hat{r})\cdot\vec{j}(\vec{r}); \qquad (2.18)$$

$j_J(qr)$ is a spherical Bessel function.

For charge and current densities we have expressions with the account of nucleon formfactor $(f_p(q^2) = f_m(q^2) = \dfrac{1}{\left(1 - \dfrac{q^2}{0.71\ \mathrm{GeV}^2}\right)^2}$; $f_n(q^2) \approx 0)$

$$\rho(\vec{r}) = \sum_{i=1}^{Z} f_p(q^2)\, \delta(\vec{r} - \vec{r}_i) + \sum_{i=1}^{N} f_n(q^2)\, \delta(\vec{r} - \vec{r}_i)\,, \tag{2.19}$$

$$\vec{j}(\vec{r}) = \sum_{i=1}^{Z} f_p(q^2) \left\{ \frac{\vec{p}_i}{2m_p}, \delta(\vec{r} - \vec{r}_i) \right\}_+ +$$

$$+ \sum_{i=1}^{N} f_n(q^2) \left\{ \frac{\vec{p}_i}{2m_n}, \delta(\vec{r} - \vec{r}_i) \right\}_+ + \vec{\nabla} \times \vec{\mu}(\vec{r})\,, \tag{2.20}$$

where $\{\ ,\ \}_+$ means anticommutator, and spin magnetic moment density is

$$\vec{\mu}(\vec{r}) = \sum_{i=1}^{Z} f_m(q^2)\, g_p \frac{\vec{\sigma}_i}{2m_p}, \delta(\vec{r} - \vec{r}_i) + \sum_{i=1}^{N} f_m(q^2)\, g_n \frac{\vec{\sigma}_i}{2m_n}, \delta(\vec{r} - \vec{r}_i)\,. \tag{2.21}$$

Inserting into (2.16—2.19) the expressions for charge and current densities we find for multipole transition operators

$$T^C_J(\vec{r}) = j_J(qr)\, Y_{J0}(\hat{r})\,, \tag{2.22}$$

$$T^E_{J\lambda}(\vec{r}) = \left[-\frac{\omega}{q} \frac{1}{\sqrt{J(J+1)}} \frac{\partial}{\partial r}(r j_J(qr)) + \frac{iq}{\sqrt{J(J+1)}} \left\{ \frac{p_r}{2m}, r j_J(qr) \right\}_+ + \right.$$

$$\left. + \frac{q}{m} \frac{1}{\sqrt{J(J+1)}}\, j_J(qr) \right] Y_{J\lambda}(\hat{r}) + \frac{1}{2} \mu_N g_N q\, j_J(qr)\, \vec{\sigma} \cdot \vec{Y}^J_{J\lambda}(\hat{r})\,; \tag{2.23}$$

$$T^M_{J\lambda}(\vec{r}) = \frac{i}{m} \sqrt{\frac{2J+1}{J+1}} \cdot \frac{j_J(qr)}{r} \vec{l} \cdot \vec{Y}^{J-1}_{J\lambda}(\hat{r}) + \frac{i}{2} \mu_N g_N q \times$$

$$\times \left(\sqrt{\frac{J+1}{2J+1}}\, j_{J-1}(qr)\, \vec{\sigma} \cdot \vec{Y}^{J-1}_{J\lambda}(\hat{r}) - \sqrt{\frac{J}{2J+1}}\, j_{J+1}(qr)\, \vec{\sigma} \cdot \vec{Y}^{J+1}_{J\lambda}(\hat{r}) \right) \tag{2.24}$$

where μ_N is nuclear magneton.

Thus, for electric transitions we have two types of tensor operators with parity $(-)^J$. We shall denote them below as t^E_i,

$$t^E_1 = Y_{J\lambda}(\hat{r})\,, \quad t^E_2 = \vec{\sigma} \cdot \vec{Y}^J_{J\lambda}(\hat{r})\,. \tag{2.25}$$

For magnetic transitions we have three types of tensor operators t^M_i with the parity $(-)^{J+1}$:

$$t^M_1 = \vec{\sigma} \cdot \vec{Y}^{J-1}_{J\lambda}(\hat{r})\,, \quad t^M_2 = \vec{\sigma} \cdot \vec{Y}^{J+1}_{J\lambda}(\hat{r})\,, \quad t^M_3 = \vec{j} \cdot \vec{Y}^{J-1}_{J\lambda}(\hat{r})\,, \tag{2.26}$$

where $\vec{j} = \vec{l} + \vec{\sigma}/2$.

3. CONTINUUM RANDOM PHASE APPROXIMATION

3.1. Shell-Model Calculations

It is convenient to start calculation in independent particle model where the wave function of final state is the simplest one. In this case

$$\psi_f = \psi^{(-)}_{k\sigma}(\vec{r})\, \tilde{\psi}_{j_h - m_h}(\vec{r}') \tag{3.1}$$

where $\tilde{\psi}_{j-m}(\vec{r})$ is the wave function of a hole, i. e. time reversed wave function of a state $\psi_{j_h m_h}(\vec{r}')$. $\psi^{(-)}_{k\sigma}(\vec{r})$ is the wave function of a final emitted nucleon, having definite momentum k and spin projection σ. For the following steps it is convenient to expand the wave function $\psi^{(-)}_{k\sigma}(\vec{r})$ over states with definite angular momentum j:

$$\psi^{(-)}_{k\sigma}(\vec{r}) = \frac{2\pi}{k} \sum_{jlm} i^l (\Omega^+_{jlm}(\hat{k}) \cdot \chi_\sigma)\, e^{-i\delta_{jl}}\, \Omega_{jlm}(\hat{r})\, R_{kjl}(r)\,. \tag{3.2}$$

Here $\Omega_{jlm}(\hat{r})$ is the spherical spinor function, and δ_{jl} are the scattering phases of a nucleon in mean-field potential of a residual nucleus. $R_{kjl}(r)$ is a single-particle radial function with the asimptotic behaviour at large distance:

$$R_{kjl}(r) \to \frac{1}{r} \sin\left(kr - \frac{\pi l}{2} + \delta_{jl} \right), \quad r \to \infty\,. \tag{3.3}$$

The matrix elements of charge and current densities (2.14, 2.15) can be written in the following way:

$$\langle f | \rho(\vec{q}) | i \rangle = \frac{2\pi}{k} \sum_{jlm} [4\pi(2J+1)]^{1/2} i^{J-l}\, e^{i\delta_{jl}} (\chi^+_\sigma \cdot \Omega_{jlm}(\hat{k})) \times$$

$$\times \langle jlm | T^C_J(q) | j_h m_h \rangle, \tag{3.4}$$

$$\langle f|J_\lambda(\vec{q})|i\rangle = \frac{2\pi}{k}\sum_{Jjlm}[2\pi(2J+1)]^{1/2} i^{J-l} e^{i\delta_{jl}} (\chi_\sigma^+ \cdot \Omega_{jlm}(\hat{k})) \times$$
$$\times \langle jlm|T^E_{J\lambda}(q) + \lambda T^M_{J\lambda}(q)|j_h m_h\rangle. \quad (3.5)$$

For longitudinal, transversal, and interference contributions to the cross-section (2.5) the following expressions can be obtained after summation over all angular momentum projections

$$\overline{|\langle f|\rho(\vec{q})|i\rangle|^2} = \sum_{I=0}^{\infty} W_I^L(q,k)\, P_I(\cos\theta_k); \quad (3.6)$$

$$\sqrt{2}\ \mathrm{Re}\left[\overline{\langle f|\rho(\vec{q})|i\rangle^* (\langle f|J_+(q) - J_-(q)|i\rangle)}\right] =$$
$$= \sum_{I=1}^{\infty} W_I^{LT}(q,k)\, P_I^1(\cos\theta_k)\, \cos\varphi_k; \quad (3.7)$$

$$\overline{|\langle f|J_+(q)|i\rangle|^2} + \overline{|\langle f|J_-(q)|i\rangle|^2} = \sum_{I=0}^{\infty} W_I^T(q,k)\, P_I(\cos\theta_k); \quad (3.8)$$

$$2\,\mathrm{Re}\left[\overline{\langle f|J_+(q)|i\rangle^* \langle f|J_-(q)|i\rangle}\right] = \sum_{I=2}^{\infty} W_I^{TT}(q,k)\, P_I^2(\cos\theta_k)\, \cos 2\varphi_k; \quad (3.9)$$

where $P_I^m(\cos\theta_k)$ is a Legendre polinomial.

The formfactors W are expressed in terms of reduced tensor operators (2.16—2.18):

$$W_I^L(q,k) = \frac{16\pi^2}{k^2}\sum_{JJ'jj'll'}\left[\frac{(2J+1)(2J'+1)}{4\pi}\right]^{1/2}\times$$
$$\times(-)^{\frac{l-l'+l'-l}{2}+j_h+j+l}\langle j'l'\|Y_l\|jl\rangle\begin{Bmatrix} l & J' & J\\ j_h & j & j'\end{Bmatrix}\times$$
$$\times C^{l0}_{J0J'0}\langle jl\|T^C_J(q)\|j_h l_h\rangle\langle j'l'\|T^C_{J'}(q)\|j_h l_h\rangle^*; \quad (3.10)$$

$$W_I^{LT}(q,k) = \frac{32\pi^2}{k^2}\sum_{JJ'jj'll'}\left[\frac{(2J+1)(2J'+1)}{4\pi l(l+1)}\right]^{1/2}\times$$
$$\times(-)^{\frac{l-l'+l'-l}{2}+j_h+j+l}\langle j'l'\|Y_l\|jl\rangle\begin{Bmatrix} l & J' & J\\ j_h & j & j'\end{Bmatrix}\times$$
$$\times C^{l1}_{J1J'0}\langle jl\|T^E_J(q) - T^M_J(q)\|j_h l_h\rangle\langle j'l'\|T^C_{J'}(q)\|j_h l_h\rangle^*; \quad (3.11)$$

$$W_I^T(q,k) = \frac{16\pi^2}{k^2}\sum_{JJ'jj'll'}\left[\frac{(2J+1)(2J'+1)}{4\pi}\right]^{1/2}\times$$
$$\times(-)^{\frac{l-l'+l'-l}{2}+j_h+j+l+1}\langle j'l'\|Y_l\|jl\rangle\begin{Bmatrix} l & J' & J\\ j_h & j & j'\end{Bmatrix}\times$$
$$\times C^{l0}_{J0J'0}\langle jl\|T^E_J(q) - T^M_J(q)\|j_h l_h\rangle\langle j'l'\|T^E_{J'}(q) - T^M_{J'}(q)\|j_h l_h\rangle^*; \quad (3.12)$$

$$W_I^{TT}(q,k) = \frac{16\pi^2}{k^2}\sum_{JJ'jj'll'}\left[\frac{(2J+1)(2J'+1)}{4\pi(l-1)\,l\,(l+1)(l+2)}\right]^{1/2}\times$$
$$\times(-)^{\frac{l-l'+l'-l}{2}+j_h+j+l+l'+1}\langle j'l'\|Y_l\|jl\rangle\begin{Bmatrix} l & J' & J\\ j_h & j & j'\end{Bmatrix}\times$$
$$\times C^{l2}_{J1J'1}\langle jl\|T^E_J(q) - T^M_J(q)\|j_h l_h\rangle\langle j'l'\|T^E_{J'}(q) + T^M_{J'}(q)\|j_h l_h\rangle^*. \quad (3.13)$$

Here $\langle j'l'\|Y_l\|jl\rangle$ is reduced matrix element of $Y_{lM}(\theta,\varphi)$ taken between states with definite total angular momentum j.

3.2. Equation for Effective Field

An interaction between quasi-particles responsible for formation of giant resonances can be taken into account in two ways. In the first way the wave function in continuum coupled with decay channels is constructed [6, 7]. In RPA the wave function is

$$|\psi^c_\omega\rangle = \sum_{ph}[X^c_\omega(ph)\, a_p^+ a_h - Y^c_\omega(ph)\, a_h^+ a_p]\,|\psi_0\rangle \quad (3.14)$$

where c is set of quantum numbers in decay channel. It includes together with total angular momentum and its projection JM the parity and quantum numbers of particle and hole.

The system of integro-differential equations for particle-hole amplitudes X^c and Y^c is formulated in coordinate representation to take into account the continuum [9].

In the second way the RPA equations are formulated for transition density operator [10, 11] and the matrix elements are defined by the integrals (2.16—2.19) where instead of charge and current densities the transition charge density and transition current density should be used. The transition density depends on single-particle quantum numbers of the exit channel as in the first approach.

This dependence can be avoided if one uses as initial and final

states the unperturbed shell-model states. In this approach the effects of particle-hole interaction are taken into account in an effective transition operator. Let us define the effective field operator in the following way:

$$\langle \psi_\omega^c | T^a | \psi_{g.s.} \rangle \equiv \langle \psi_\omega^0 | V^a | \psi_0 \rangle \tag{3.15}$$

where $a=(C, E, M)$, and $|\psi^0\rangle$ is a shell-model state used in (3.4, 3.5). Let H_0 be shell-model Hamiltonian and W the residual interaction. The state $|\psi_\omega^c\rangle$ is coupled with corresponding shell-model state by the equation

$$|\psi_\omega^c\rangle = \left(1 - \frac{1}{-E_c + H_0 + W} W\right) |\psi_\omega^0\rangle, \tag{3.16}$$

from (3.15) and (3.16) one obtains the equation coupling effective field and external field operators

$$V^a = \left(1 - W \frac{1}{H_0 + W - E_c}\right) T^a \left(1 - \frac{1}{H_0 + W - E_c} W\right); \tag{3.17}$$

reversing the equation one has

$$T^a = \left(1 - W \frac{1}{H_0 - E_c}\right) V^a \left(1 + \frac{1}{H_0 - E_c} W\right); \tag{3.18}$$

or

$$V^a = T^a - W \frac{1}{H_0 - E_c} V^a - V^a \frac{1}{H_0 - E_0} W - W \frac{1}{H_0 - E_c} V^a \frac{1}{H_0 - E_0} W. \tag{3.19}$$

The state $|\psi_\omega^0\rangle$ is the one of particle-hole type. Omitting the last term in (3.19) one can obtain the RPA equation by retaining in intermediate states in r.h.s of (3.19) the states of particle-hole type as well. The second term in r.h.s. of (3.19) describes propagation of a particle and a hole interacting in a final state. The third term in r.h.s. of (3.19) accounts for ground state correlations. The last term in (3.19) omitted for symplicity leads to renormalization of residual interaction W to the effective one.

It is convenient to draw the Eq. (3.19) in graphs. In Fig. 2 $(a-e)$ the graphs corresponding to each term of r.h.s. of (3.19) are shown. There are several graphs for renormalization of residual interaction and only one of them is shown as an example in Fig. 2,*e*. Introducing now the Feinman propagator of quasi-particle G one can write down our equation in a unified form (see Fig. 3):

$$V^a = T^a + FGGV^a, \tag{3.20}$$

where F is the effective quasi-particle interaction. This interaction is choosen in Landau—Migdal form:

$$F(\vec{r}, \vec{r}') = C\delta(\vec{r} - \vec{r}')[f + f'\vec{\tau}_1 \cdot \vec{\tau}_2) + g(\vec{\sigma}_1 \cdot \vec{\sigma}_2) + g'(\vec{\sigma}_1 \cdot \vec{\sigma}_2)(\vec{\tau}_1 \cdot \vec{\tau}_2)], \tag{3.21}$$

where the normalization constant $C = 300$ MeV·fm^3 [19]. The interaction constants f, f', g, g' are, strictly speaking, functions of density. This dependence is important, however, only for the constant f, and we write it in conventional form [19]:

$$f = f_{in} - (f_{ex} - f_{in}) \frac{\rho(r) - \rho(0)}{\rho(0)}, \tag{3.22}$$

where

$$\rho(r) = \frac{\rho_0}{1 + \exp\left(\frac{r - R}{a}\right)}. \tag{3.23}$$

For local interaction (3.21) the effective fields V^a are coordinate functions. For spherical nucleus it is convenient to separate an angular dependence in $V^a(\vec{r})$ expanding it over set of tensor operators. The expansion is for electric transitions:

$$V^E(\vec{r}) = \sum_{j=1,2} V_j^E(r)\, t_j^E + i \frac{q}{\sqrt{J(J+1)}} \left\{ \frac{p_r}{2m}, r j_J(qr) \right\}_+ t_1^E; \tag{3.24}$$

for magnetic transitions:

$$V^M(\vec{r}) = \sum_{j=1,2} V_j^M(r)\, t_j^M + i \frac{1}{m} \sqrt{\frac{2J+1}{J+1}}\, \frac{j_J(qr)}{r}\, t_3^M; \tag{3.25}$$

for Coulomb transitions:

$$V^C(\vec{r}) = \sum_{j=1,2} V_j^C(r)\, t_j^E. \tag{3.26}$$

The expansion of the interaction (3.21) in a series of tensor operators (2.25, 2.26) has no contribution of the operator t_3^M, and interaction (3.21) is momentum independent. For these reasons the last terms in (3.24, 3.25) are not renormalized by particle-hole interaction (3.21).

Inserting (3.24, 3.25) in (3.20) we obtain a system of integral equations for the components $V_i^E(r)$ or $V_i^M(r)$:

$$V_j^E(r) = T_j^E(r) + F_j \int dr' A_{ji}^E(r, r'; \omega) V_i^E(r') + B_j^E(r), \qquad (3.27)$$

$$V_j^M(r) = T_j^M(r) + F_j \int dr' A_{ji}^M(r, r'; \omega) V_i^M(r') + B_j^M(r), \qquad (3.28)$$

where $T_j^a(r)$ are the «bare» components of the fields (2.22—2.24), and $B_j^a(r)$ is additional r.h.s. arising due to admixture in components with $i=1, 2$ nonrenormalizable parts of (3.24, 3.25). Explicit expressions for A_{ji}^a and B_j^a can be found in Appendix.

Above nucleon emission threshold the kernels A_{ji} become complex acquiring imaginary part. At these energies the effective fields become complex as well. This is the main difference in our approach from the one used in Ref. [11] where they start with equations for transition densities using the real part of the kernels A_{ji}.

The system of Eqs (3.27, 3.28) has been solved numerically in the following way. The kernels A_{ji} were calculated in coordinate points with mesh 0.2 fm. The effective field V^a as more smooth function had a mesh 0.4 fm and linear interpolation was used for intermediate points. Integration in (3.27, 3.28) has been performed up to 8 fm. At larger distance the effective field has been taken equal to the external one.

3.3. Separation of the Center of Mass Motion

Calculating the cross-section for E1-multipolarity it is important to separate excitation of a «ghost» mode. In our case this is the center of mass displacement mode. Due to linearity of RPA equations it is sufficient to exclude its excitation from the «bare» external field. The effective field will not contain it automatically.

For charge density the bare operator (2.16) is not invariant under translation. The correct translation-invariant operator is

$$\rho(\vec{q}) = \sum_{j=1}^{Z} e^{i\vec{q}(\vec{r}_j - \vec{R})} \qquad (3.29)$$

where $\vec{R}$ is the center of mass coordinate. Expanding (3.29) in series of $\vec{q}\cdot\vec{R}$ and retaining only first term contributing to E1-transition one has

$$\rho(\vec{q}) = \sum_{j=1}^{Z} e^{i\vec{q}\vec{r}_j} - \frac{\vec{q}}{A} \sum_{n=1}^{A} \vec{r}_n \sum_{j=1}^{Z} e^{i\vec{q}\vec{r}_j}. \qquad (3.30)$$

One has to calculate matrix element from ground state $|0\rangle$ to excited state $|\omega\rangle$. In RPA

$$\langle\omega| \sum_{n=1}^{A} \frac{\vec{q}\cdot\vec{r}_n}{A} \cdot \sum_{j=1}^{Z} e^{i\vec{q}\vec{r}_j} |0\rangle \approx \frac{\vec{q}}{A} \langle\omega| \sum_{n=1}^{A} \vec{r}_n |0\rangle \langle 0| \sum_{j=1}^{Z} e^{i\vec{q}\vec{r}_j} |0\rangle =$$

$$\frac{F(\vec{q})}{A} \vec{q} \langle\omega| \sum_{n=1}^{A} \vec{r}_n |0\rangle, \qquad (3.31)$$

thus, at finite momentum transfer q instead of factor Z/A, known from photoreactions, the factor $F(\vec{q})/A$ appeared where $F(\vec{q})$ is the normalized on Z charge formfactor of a nucleus.

This result looks very natural. At large momentum transfer q interaction between virtual γ-quantum and a nucleon becomes more local and influence of a center of mass motion must disappear. In other words the effective proton charge equal $1 - F(\vec{q})/A$ tends to 1 at $\vec{q} \to \infty$. The effective charge of a neutron is then $-F(\vec{q})/A$.

For the current density the subtraction is performed in a similar way. In this case the subtracted operator is the total momentum of a nucleus.

4. RESULTS AND DISCUSSION

4.1. Single-Particle and Particle-Hole Interaction Parameters

To reproduce right positions of giant resonances it is important to reproduce first the single-particle energies. We used the Woods—Saxon single-particle potential

$$U(r) = -U_0 f(r) + U_{l.s.} \vec{\sigma}\cdot\vec{l} \left(\frac{\hbar}{m_\pi c}\right)^2 \frac{1}{r} \frac{df(r)}{dr} + U_{\text{Coul}}(r) \qquad (4.1)$$

where

$$f(r) = \frac{1}{1 + \exp\left(\frac{r-R}{a}\right)}. \qquad (4.2)$$

For protons the Coulomb term must be added

$$U_{\text{Coul}}(r) = \begin{cases} \frac{3}{2}\,\frac{Ze^2}{R}\left(1-\frac{r^2}{3R^2}\right) & r \leqslant R \\ \frac{Ze^2}{r} & r > R \end{cases} \qquad (4.3)$$

Strictly speaking, the potential (4.1) does not reproduce accurately enough the positions of p and d levels in ^{16}O. Therefore, we used state dependent potential from Ref. [20]. The parameters of the potential are listed in Table 1. For all parts of potential radius $R=3.08$ fm. and diffuseness $a=0.53$ fm. For $1s_{1/2}$ level which is not known accurately enough from experiment we used the same parameters as for $2s_{1/2}$ level. For states in continuum parameters were not changed in order to keep them orthogonal to bounded states. For angular momentum $L>2$, $U_0=50$ MeV and $U_{l.s.}=7$ MeV.

Table 1

Potential Parameters from Fit of Single-Particle Energies of ^{16}O

State	Protons			Neutrons		
	E (MeV)	U_0 (MeV)	$U_{l.s.}$ (MeV)	E (MeV)	U_0 (MeV)	$U_{l.s.}$ (MeV)
$1p_{1/2}$	−12.12	57.95	9.89	−15.64	57.39	9.64
$1p_{3/2}$	−18.44			−21.80		
$1d_{3/2}$	+4.50	54.36	5.27	+0.94	54.94	5.27
$1d_{5/2}$	−0.60			−3.27		
$2s_{1/2}$	−0.10	55.91	—	−4.14	56.82	

Table 2

Parameters of Particle-Hole Interaction

C (MeV·fm^3)	R (fm)	a (fm)	f_{in}	f_{ex}	f'	g	g'
300	2.71	0.60	0.214	−2.235	1.3	0.4	0.6

The parameters of effective interaction are listed in Table 2. The values of isoscalar constants f and f' were found from fit of the position of the displacement «ghost» mode and position of 3^- level at

6.13 MeV. The value of isovector constant f' was found by fitting the position of main peak of giant dipole resonance. The values of isoscalar constants appeared to be close to those used for heavier nuclei (see [19]). The parameter f' is 30% greater than usual and this is consistent with results of Ref. [11].

The results are least sensitive to the constants g and g' and we used the values from Ref. [13].

4.2. The (γ, N) Reaction

The nucleon spectra from (γ, N) reaction for different values of constant f' are shown in Figs 4 and 5. An increase of the f' does not change appreciably the position of main peak but increases considerably the width of the peak decreasing thus its height. With the increase of f' the transition strength is shifted up to higher excitation energies rising the right wing and plato behind the resonance. Peaks at lower energies are mostly sensitive to single-particle energies. Most of them correspond to spin-flip transitions therefore their height depends on spin-spin constants g and g'.

The comparison of calculated curves with the experiment taken from review paper [20] shows the general shape of a spectrum is reproduced in RPA correctly. The difference appears in fine structure of the giant resonance peaks. The fine structure indicates the presence of more complex than $1p-1h$ configurations in the wave function of a resonance.

The total absorption cross-section of γ-quanta is shown in Fig. 6. It has similar level of agreement with experiment compared to the cross-sections in separate channels.

4.3. The $(e, e'N)$ Reaction

The contribution of separate multipole transitions in the proton spectrum in the reaction $(e, e'p_0)$ are shown in Figs 7 and 8.

At electron energy $E=130$ MeV and electron scattering angle $\theta=53.1°$ the momentum transfer $q\approx 0.5$ fm^{-1} and it is varying slowly with ω [5]. In this case $qR\approx 1.4$, i. e. it is several times greater than for (γ, N) reaction. Nevertheless, the main contribution to the cross-section comes from the E1-transition. Contribution of $J=2, 3$ multipolarities is important only near corresponding resonances (see Fig. 7). The E0-transition in ^{16}O in RPA does not show resonant behaviour and its strength is distributed in the energy

region 15—25 MeV. The transition with $J=4$ has no resonances as well and contribution of higher multipolarities can be neglected.

The main feature of E2-transition is the existance of huge giant quadrupole peak at the energy $E=23.5$ MeV. Nothing comparable to such peak is seen in experimental spectra. The appearance of this peak is in fact a drawback of the approximation used. In RPA the main contribution to the E2-resonance comes from the single-particle transition between $1s_{1/2}$ and $1d_{5/2}$ states both with negative energy. The coupling with continuum and, therefore, the width arises in higher order in residual interaction. This explains small resulting width and big height of a resonance. In real situation deep hole state $1s_{1/2}$ has big spreading width and its contribution to E2-resonance is suppressed. Fig. 8 shows strength distribution of the E2-transition when contribution of the level $1s_{1/2}$ is absent. In this case the position of the resonance is shifted to higher energy and its height is much smaller.

The total spectrum with contribution of the multipolarities up to $J=4$ is shown in Fig. 9. As for the (γ, N) reaction the calculated cross-sections are less structured and slightly higher than the measured ones due to absence of more complex than $1p-1h$ configurations. In addition, the E2-resonance is more strong in our calculations in comparison with measured spectrum.

The spectra for the $(e, e'p_1)$, $(e, e'n_0)$ and $(e, e'n_1)$ reactions are shown in Figs 10, 11, 12.

4.4. Angular Distributions

In Figs 13 and 14 proton angular distributions are shown for two different excitation energy regions. In the resonance region, as expected from differences in calculated and measured [5] spectra, the angular distributions are reproduced in calculations rather poorly. They depend strongly on details of strength distribution of different multypolarities (Fig. 13). At higher excitation energy the resonances disappear and transition strength depends smoothly on the energy. The contributions of multipolarities higher then $J=1$ become comparable to contribution of the dipole transition leading to strong asymmetry of angular distributions along q direction. At high q such anisotropy would be indication of quasi-free knockout process. However, at our value of $q\simeq 100$ MeV/c recoil energy of a nucleon is about 5 MeV only. It is well below of nucleon emission threshold $E_{th}=12.2$ MeV. It is therefore possible to think only about

far tail of a quasi-free process and some traces of it are kept in coherent contribution of different multipolarities at forward direction. Certainly the agreement in angular distributions is better in this region.

The authors are grateful to P.N. Isaev who took part in initial stage of the work to V.G. Zelevinsky, S.G. Popov and B.B. Voitsekhovsky for numerous discussions of the results.

APPENDIX

The effective interaction (3.21) can be expanded in the set of tensor operators (2.25, 2.26)

$$F(\vec{r},\vec{r}')=C\sum_{JM}[(f(r)+f'(\vec{\tau}_1\cdot\vec{\tau}_2))\,t_1^E(\hat{r})\,t_1^{E^-}(\hat{r}')+(g+g'(\vec{\tau}_1\cdot\vec{\tau}_2))\times$$

$$\times(t_2^E(\hat{r})\,t_2^{E^+}(\hat{r}')+t_1^M(\hat{r})\,t_1^{M^-}(\hat{r}')+t_2^M(\hat{r})\,t_2^{M^+}(\hat{r}'))]\,\frac{1}{r^2}\delta(r-r')\,. \qquad (A.1)$$

Using the expansion (3.24—3.26) for effective fields one obtains after separation of reduced matrix elements of the tensor operators (2.25, 2.26)

$$V_i^a(r)=T_i^a(r)+F_i^a\int r'^2\,dr'\,B_{ij}^a(r,r';\omega)\,T_j^a(r')+F_i^a\int r'^2\,dr'\,A_{ij}^a(r,r';\omega)\,V_j^a(r') \qquad (A.2)$$

where F_i^a is a matrix in isotopical space:

$$F_1^E=f+f'(\vec{\tau}_1\cdot\vec{\tau}_2)\,;\qquad F_2^E=F_i^M=g+g'(\vec{\tau}_1\cdot\vec{\tau}_2)\,;$$

and

$$A_{ij}^a(r,r';\omega)=\frac{1}{2J+1}\sum_{\nu\nu'}(j_{\nu'}\,l_{\nu'}\|t_i^a\|j_\nu\,l_\nu)\,(j_{\nu'}\,l_{\nu'}\|t_j^a\|j_\nu\,l_\nu)\,R_\nu(r)\,R_{\nu'}(r)\times$$

$$\times\frac{n_\nu-n_{\nu'}}{\varepsilon_\nu-\varepsilon_{\nu'}+\omega-i\delta\frac{\omega}{|\omega|}}\,R_{\nu'}(r')\,R_\nu(r')\,. \qquad (A.3)$$

Introducing the Green function of a radial Schrödinger equation one has for electric transitions

$$A_{ij}^E(r,r';\omega)=\frac{1}{2J+1}\sum_{\nu\nu'}(j_{\nu'}\,l_{\nu'}\|t_i^E\|j_\nu\,l_\nu)\,(j_{\nu'}\,l_{\nu'}\|t_j^E\|j_\nu\,l_\nu)\,n_\nu\times$$

$$\times[\,G_{\nu'}(r,r'|\varepsilon_\nu+\omega)+(-)^{i+j}G_{\nu'}(r,r'|\varepsilon_\nu-\omega)]\,R_\nu(r)\,R_\nu(r')\,, \qquad (A.4)$$

nd for magnetic transitions

$$A^M_{ij}(r,r';\omega)=\frac{1}{2J+1}\sum_{\nu\nu'}(j_{\nu'}\,l_{\nu'}\|t^M_i\|j_\nu\,l_\nu)\,(j_{\nu'}\,l_{\nu'}\|t^M_j\|j_\nu\,l_\nu)\,n_\nu\times$$

$$\times[\,G_{\nu'}(r,r'|\varepsilon_\nu+\omega)+G_{\nu'}(r,r'|\varepsilon_\nu-\omega)]\;R_\nu(r)R_\nu(r')\,. \qquad (A.5)$$

For B^a_{ij} one has: for electric transitions

$$B^E_{ij}(r,r';\omega)=\frac{\delta_{j1}}{2J+1}\sum_{\nu\nu'}(j_{\nu'}\,l_{\nu'}\|t^E_i\|j_\nu\,l_\nu)\,(j_{\nu'}\,l_{\nu'}\|t^E_j\|j_\nu\,l_\nu)\;R_\nu(r)R_{\nu'}(r)\times$$

$$\times\frac{n_\nu-n_{\nu'}}{\varepsilon_\nu-\varepsilon_{\nu'}+\omega-i\delta\frac{\omega}{|\omega|}}\left(R_{\nu'}(r')\frac{dR_\nu(r')}{dr'}-\frac{dR_{\nu'}(r')}{dr'}R_\nu(r')\right). \qquad (A.6)$$

or

$$B^E_{ij}(r,r';\omega)=\frac{\delta_{j1}}{2J+1}\sum_{\nu\nu'}(j_{\nu'}\,l_{\nu'}\|t^E_i\|j_\nu\,l_\nu)\,(j_{\nu'}\,l_{\nu'}\|t^E_j\|j_\nu\,l_\nu)\,n_\nu\times$$

$$\times\Big\{R_\nu(r)\frac{dR_\nu(r')}{dr'}|\;G_{\nu'}(r,r'|\varepsilon_\nu+\omega)+(-)^iG_{\nu'}(r,r'|\varepsilon_\nu-\omega)]-$$

$$-R_\nu(r)R_\nu(r')\Big[\frac{\partial G_{\nu'}(r,r'|\varepsilon_\nu+\omega)}{\partial r'}+(-)^i\frac{\partial G_{\nu'}(r,r'|\varepsilon_\nu-\omega)}{\partial r'}\Big]\Big\}. \qquad (A.7)$$

For magnetic transitions

$$B^M_{ij}(r,r';\omega)=\delta_{j3}\,A^M_{i3}(r,r';\omega)\,. \qquad (A.8)$$

The Green function $G(r,\,r'|E)$ of a radial Schrödinger equation has been calculated using two independent solutions the one regular at $r=0$ and the other regular at infinity

$$G_\nu(r,r'|E)=\frac{2m}{\hbar^2}\;\frac{y^{(1)}_\nu(r_<)\,y^{(2)}_\nu(r_>)}{W} \qquad (A.9)$$

where W is the Wronskian of these two solutions.

REFERENCES

1. *G.I. Budker et al.* Yadernaya Fizika, 6 (1967) 775.
2. *M. Bernheim et al.* Nucl. Phys. A375 (1982) 381.
3. *P.K.A. De Witt Huberts.* Nucl. Phys. A446 (1985) 301c.
4. *J. Ahrens et al.* Nucl. Phys. A251 (1975) 479.
5. *V.F. Dmitriev et al.* Nucl. Phys. A464 (1987) 237.
6. *V.V. Balashov, N.M. Kabachnik and V.I. Markov.* Nucl. Phys. A129 (1969) 369.
7. *B. Kämpfer and R. Wünsch.* Nucl. Phys. A426 (1984) 301.
8. *H. Feshbach.* Ann. Phys. 19 (1962) 287.
9. *M. Cavinato, M. Marangoni, P.L. Ottaviani and A.M.Saruis.* Nucl. Phys. A373 (1982) 445.
10. *R. de Haro, S. Krewald and J. Speth.* Nucl. Phys. A338 (1982) 265.
11. *G. Co' and S. Krewald.* Nucl. Phys. A433 (1985) 392.
12. *S. Shlomo and G. Bertsch.* Nucl. Phys. A243 (1975) 507.
13. *V.F. Dmitriev and V.B. Telitsin.* Nucl. Phys. A402 (1983) 581.
14. *T. de Forest, Jr.* Ann. Phys. 45 (1967) 365.
15. *W.E. Kleppinger and J.D. Walecka.* Ann. Phys. 146 (1983) 349.
16. *D. Drechsel and H. Überall.* Phys. Rev. 181 (1969) 1383.
17. *D.A. Warshalovitch, A.N. Moskalev, W.K. Khersonsky.* Quantum Theory of Angular Momentum. — Leningrad, Nauka, 1975.
18. *L.D. Landau and E.M. Lifshits.* Theory of Field. — Moscow, Nauka, 1973.
19. *A.B. Migdal.* Theory of Finite Fermi-System and Properties of Atomic Nuclei. — Moscow, Nauka, 1983.
20. *B. Buck and A.D. Hill.* Nucl. Phys. A95 (1967) 271.
21. *F. Fuller.* Phys. Rep. 127 (1985) 185.

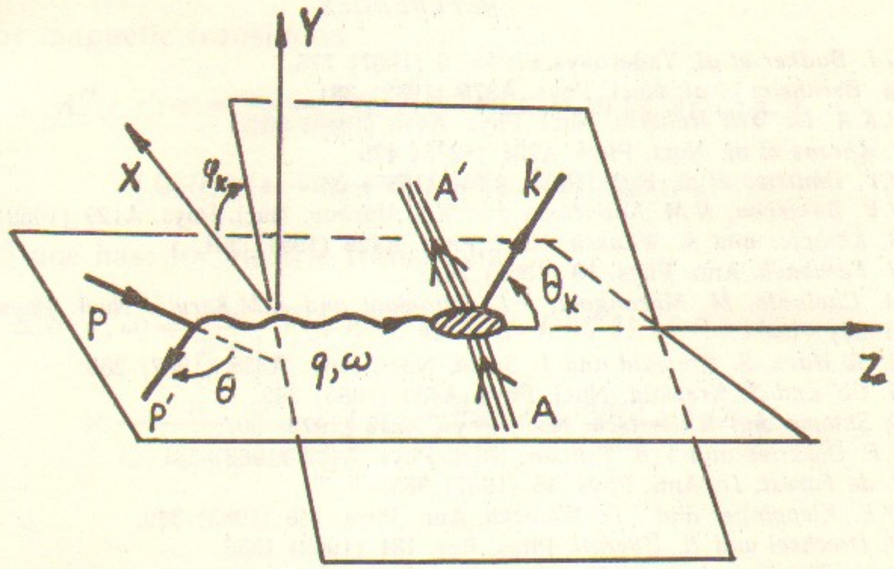

Fig. 1. Kinematics of the $(e, e'N)$ reaction in one-photon approximation.

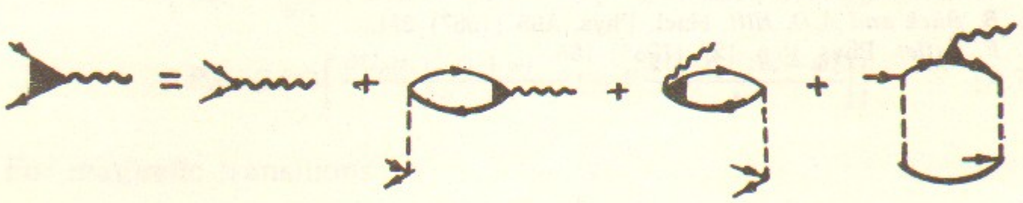

Fig. 2. Graphs, corresponding to the Eq. (3.19) for the effective field:
a — the effective field; *b* — the bare field; *c* — propagation of interacting particle and hole in a final state; *d* — ground-state correlations; *e* — renormalization of initial interaction.

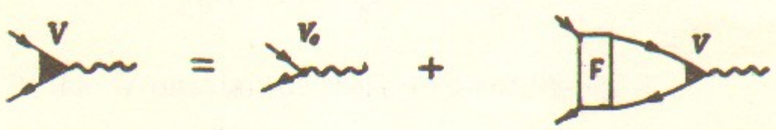

Fig. 3. Feinman diagramms for effective field equation.

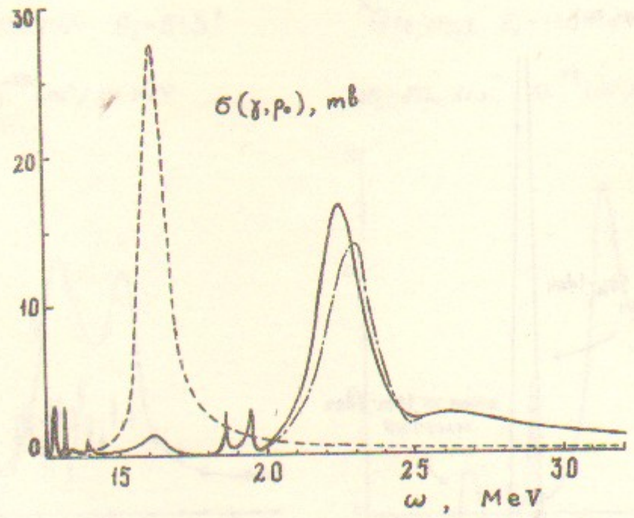

Fig. 4. Proton spectrum in (γ, p_0) reaction for different values of the constant f'. The full line — $f'=1.3$; dash-dotted line — $f'=1.5$; dashed line — the spectrum in absence of interaction.

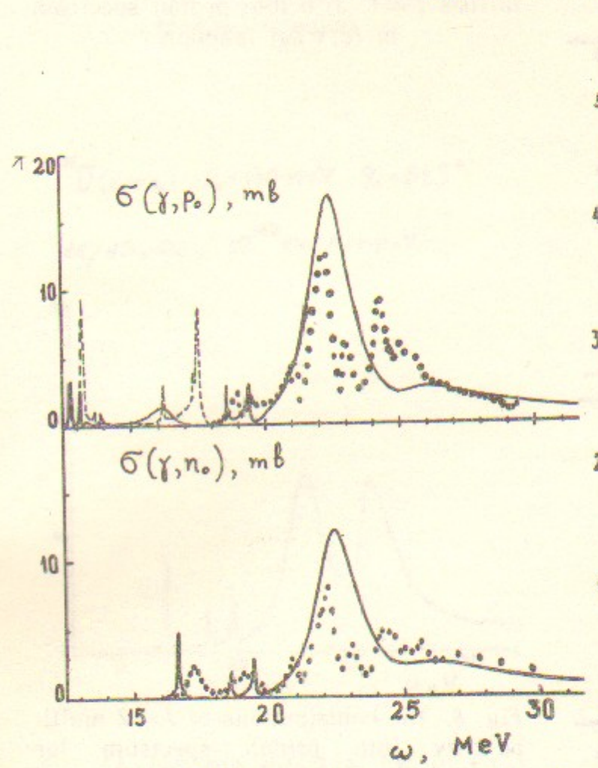

Fig. 5. Proton and neutron spectra in (γ, N_0) reaction. Full line presents theoretical calculation, dotts and dashed line are mesurements.

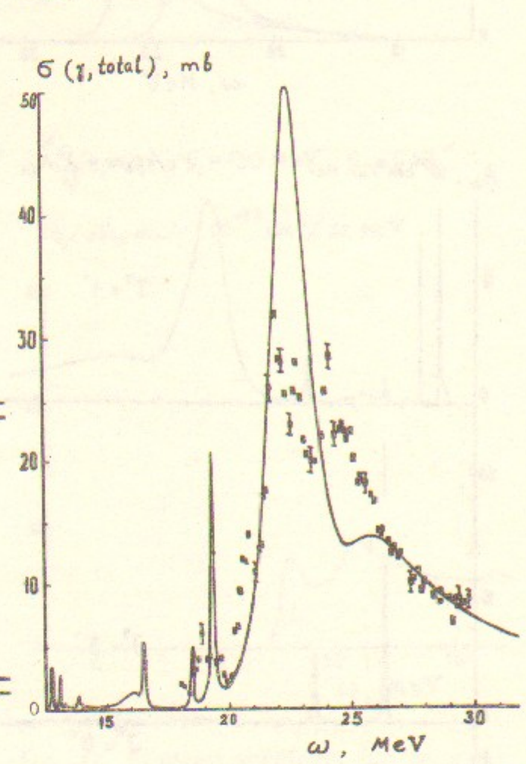

Fig. 6. Total absorption cross-section of γ-quanta in ^{16}O.

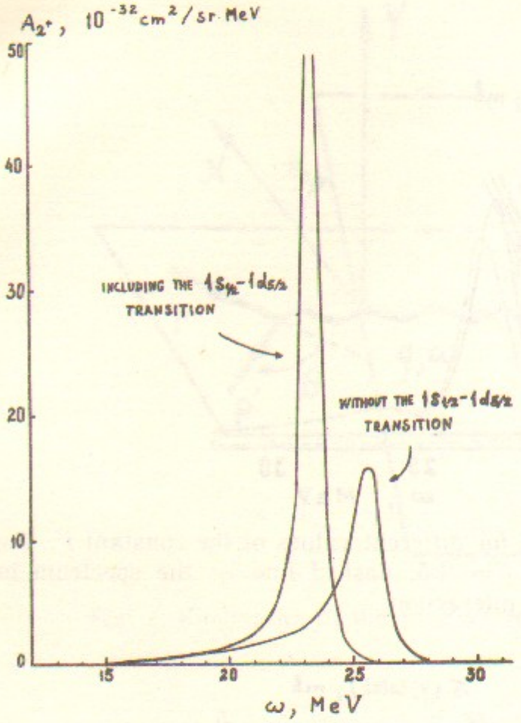

Fig. 7. Partial contributions of multipolarities $J=1$, 3, 0 into proton spectrum in $(e, e'p_0)$ reaction.

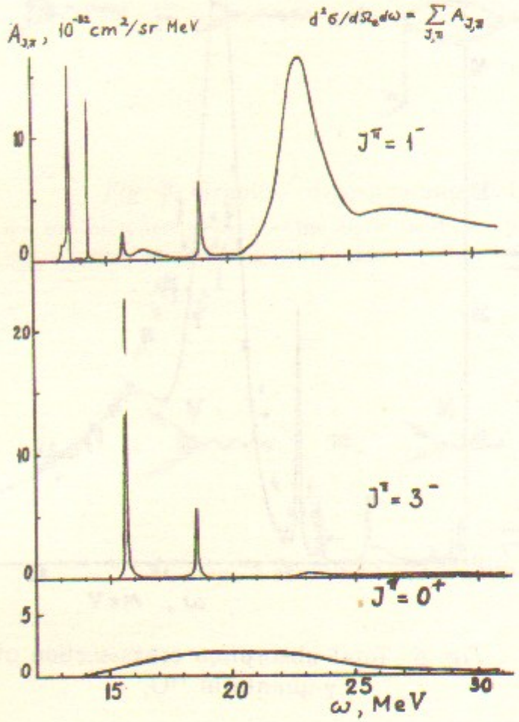

Fig. 8. The contributions of $J=2$ multipolarity into proton spectrum for $(e, e'p_0)$ reaction with account of $1s_{1/2}-1d_{5/2}$ transition and suppressing it.

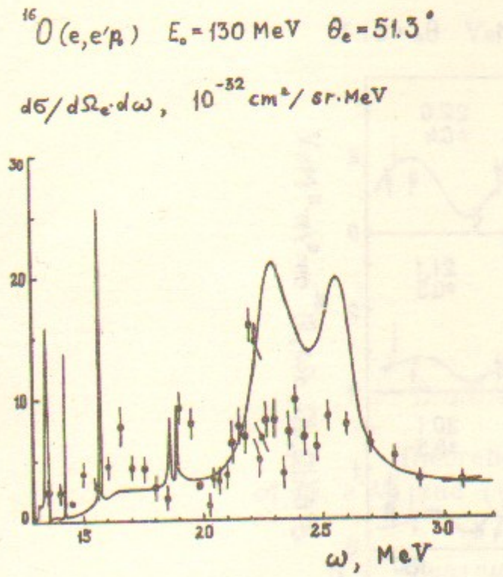

Fig. 9. Full proton spectrum for $(e, e'p_0)$ reaction.

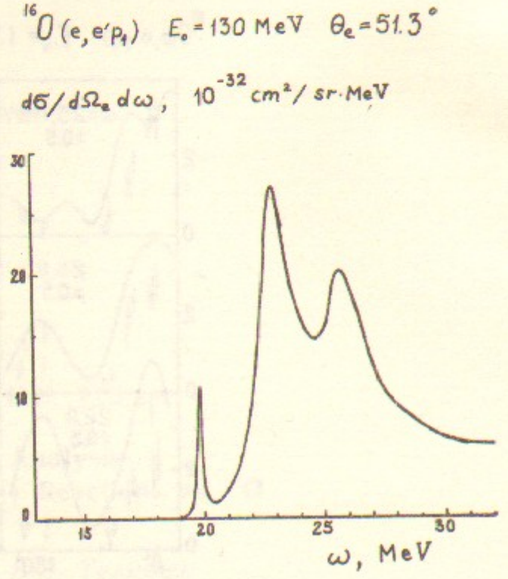

Fig. 10. Proton spectrum for $(e, e'p_1)$ reaction.

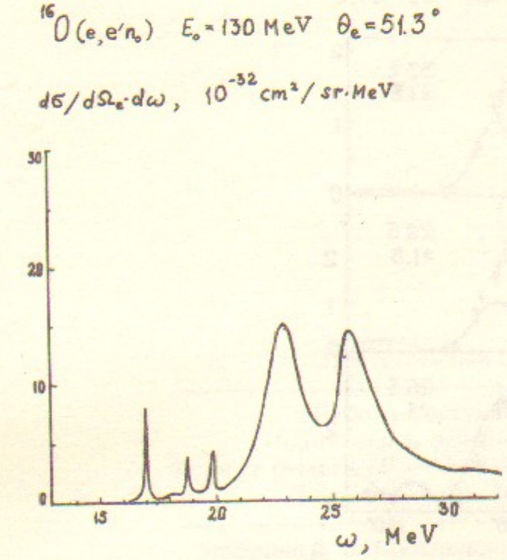

Fig. 11. Neutron spectrum for $(e, e'n_0)$ reaction.

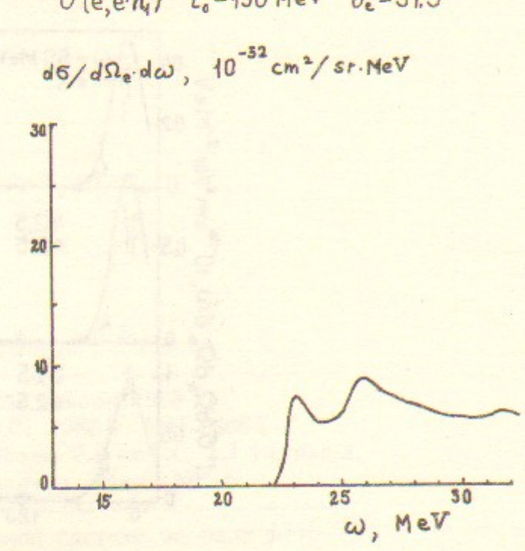

Fig. 12. Neutron spectrum for $(e, e'n_1)$ reaction.

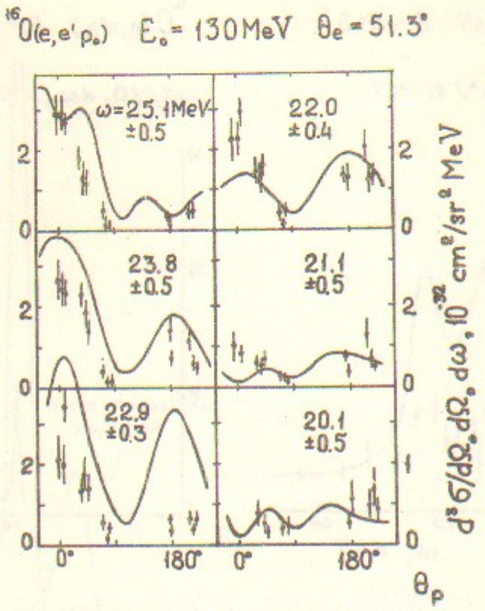

Fig. 13. Proton angular correlations for $(e, e'p_0)$ reaction in the resonance region.

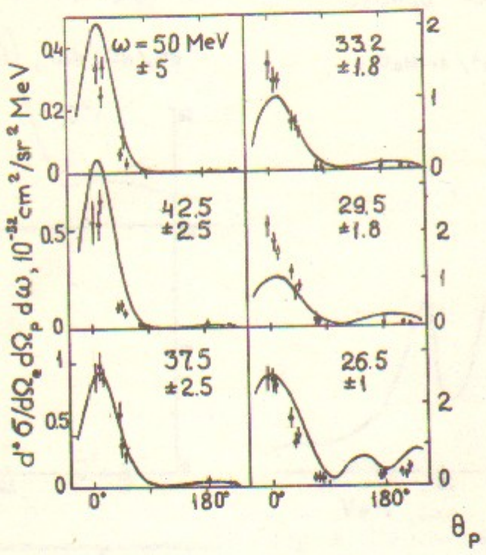

Fig. 14. Proton angular correlations for $(e, e'p_0)$ reaction in the energies behind resonance region.

V.F. Dmitriev, V.B. Telitsin

Theoretical Analysis of $(e, e'N)$ and (γ, N) Reactions on ^{16}O

В.Ф. Дмитриев, В.Б. Телицын

Теоретический анализ реакций $(e, e'N)$ и (γ, N) на ^{16}O

Ответственный за выпуск С.Г.Попов

Работа поступила 20 января 1988 г.
Подписано в печать 29.01 1988 г. МН 08083
Формат бумаги 60×90 1/16 Объем 2,8 печ.л., 2,3 уч.-изд.л.
Тираж 250 экз. Бесплатно. Заказ № 15

Набрано в автоматизированной системе на базе фотонаборного автомата ФА1000 и ЭВМ «Электроника» и отпечатано на ротапринте Института ядерной физики СО АН СССР,
Новосибирск, 630090, пр. академика Лаврентьева, 11.